Journal of Applied Polymer Science

Preparation of a Chitosan-Based Flame-Retardant Synergist and Its Application in Flame-Retardant Polypropylene

Youyou Xiao,[1] Yuying Zheng,[1] Xie Wang,[2] Zhijie Chen,[1] Zhe Xu[1]
[1]College of Materials Science and Engineering, Fuzhou University, Fuzhou 350116, China
[2]College of Chemistry and Chemical Engineering, Fuzhou University, Fuzhou 350116, China
Correspondence to: Y. Zheng (E-mail: yyzheng@fzu.edu.cn)

ABSTRACT: A novel flame-retardant synergist, chitosan/urea compound based phosphonic acid melamine salt (HUMCS), was synthesized and characterized by Fourier transform infrared spectroscopy and ^{31}P-NMR. Subsequently, HUMCS was added to a fire-retardant polypropylene (PP) compound containing an intumescent flame-retardant (IFR) system to improve its flame-retardant properties. The PP/IFR/HUMCS composites were characterized by limiting oxygen index (LOI) tests, vertical burning tests (UL-94 tests), microscale combustion calorimetry tests, and thermogravimetric analysis to study the combustion behavior and thermal stability. The addition of 3 wt % HUMCS increased the LOI from 31.4 to 33.0. The addition of HUMCS at a low additive amount reduced the peak heat-release rate, total heat release, and heat-release capacity obviously. Furthermore, scanning electron micrographs of char residues revealed that HUMCS could prevent the IFR–PP composites from forming a dense and compact multicell char, which could effectively protect the substrate material from combusting. © 2014 Wiley Periodicals, Inc. J. Appl. Polym. Sci. **2014**, *131*, 40845.

KEYWORDS: flame retardance; synthesis and processing; thermal properties

Received 20 November 2013; accepted 7 April 2014
DOI: 10.1002/app.40845

INTRODUCTION

Polypropylene (PP) has been widely used in many fields, including electrical and transport applications and household materials in general.[1] However, its wider application is restricted by its inherent combustibility. Therefore, it is essential to endow PP with a good flame retardancy.[2,3]

Intumescent flame-retardants (IFRs) are one of the most widely used halogen-free flame retardants because of their numerous advantages, including a high efficiency and low toxicity.[4,5] It is well known that a typical IFR is composed of three ingredients, namely, an acid source, such as phosphate; a carbon source, commonly pentaerythritol (PER); and a blowing agent, such as melamine (MA).[6] The IFR system is characterized by its intense expansion and the formation of multicellular charred layers, which protect the underlying substrate material well from the attack of flames and oxygen during combustion.[7] The multicellular foam also protects the substrate from heat. Therefore, the carbon agent, which affects the formation of char, plays an essential role in the intumescent system.[8] However, it is urgent to develop new sustainable carbon agents because availability and cost for PER will show a worse trend.

Over the past few years, there has been enormous attention on the use of chitosan (CS). CS is obtained by the alkaline deacetylation of chitin, which is a very abundant naturally occurring polymeric material.[9,10] Meanwhile, CS is an amino polysaccharide with the structure of multihydroxyl groups; this makes it a potential and promising green carbon agent.[11] However, the poor solubility of CS in common solvents has been a major drawback in its utilization.[12] In previous works,[13,14] strong acids have been used as a solvent to dissolve CS, such as methanesulfonic acid. Nevertheless, a simple and easy way to prepare a CS-based flame retardant is needed for industrialized production.

Some efforts have been made to investigate the interactions between urea and CS in aqueous solution. According to Chenite et al.,[15] CS can be water-soluble under acidic conditions that provide sufficient protonation of its amino groups. Tsaih and Chen[16] demonstrated that urea can reduce the attractive interchain hydrogen bonding of CS and hydrophobic forces. Sogias et al.[12] introduced a physical approach to expand the solubility window of CS. They concluded that the precipitation point of CS shifted to pH 8.0 in the presence of 8 mol/L urea. A subsequent study of this group showed that urea promoted the solubility of CS in an aqueous solution. Many reports on the application of solutions of CS and urea have been reported.[17,18] However, to the best of our knowledge, there have been no reports on the use of CS/urea solutions to prepare flame-retardant compounds. Herein, urea was chosen as an

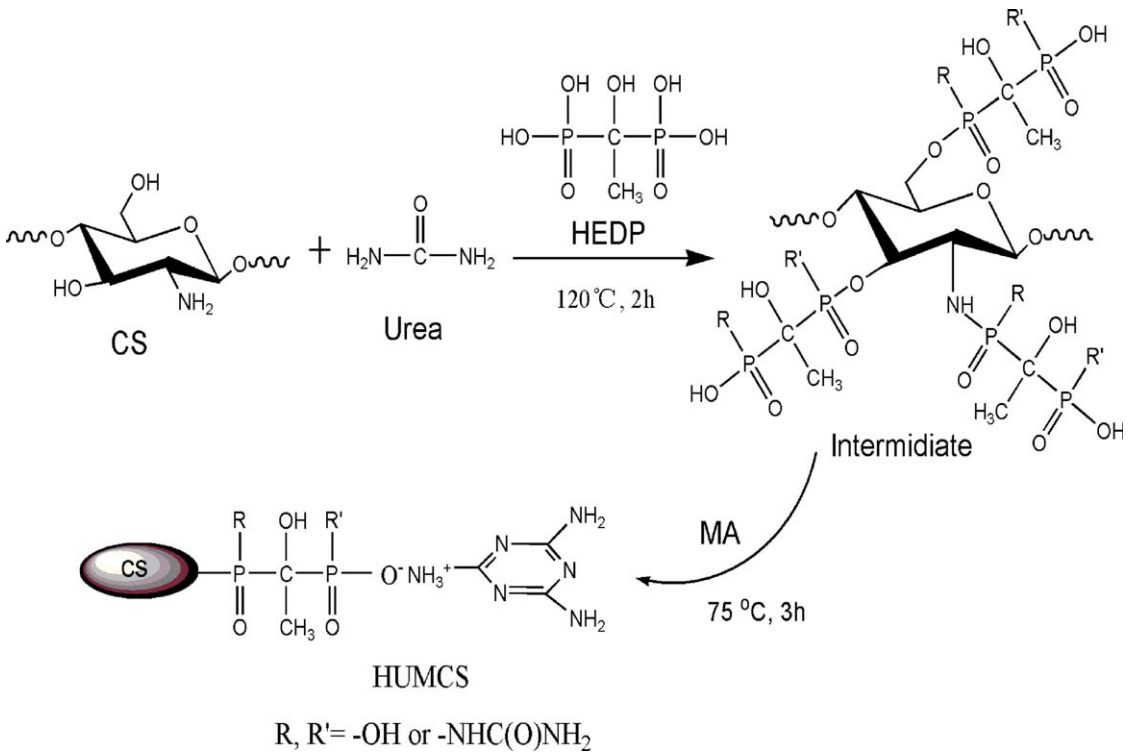

Scheme 1. Synthetic route of HUMCS. [Color figure can be viewed in the online issue, which is available at wileyonlinelibrary.com.]

accelerating agent to expand the solubility window of CS because urea can also be used as a blowing agent in flame-retardant compounds.

In this study, novel chitosan/urea compound based phosphonic acid melamine salt (HUMCS) was prepared in aqueous solution via 1-hydroxy ethylidene-1,1-diphosphonic acid (HEDP), urea, MA, and CS. Then, it was added to PP in addition to an IFR system. The synergistic effect between HUMCS and IFR was studied. The tensile properties of the PP/IFR/HUMCS composites and the morphology of the residual char were also investigated. Through this investigation, we expected to make use of the CS/urea solution to prepare an efficient CS-based flame-retardant synergist in an aqueous solution.

EXPERIMENTAL

Materials

Commercial PP (TS30) was obtained from Fujian Petroleum Chemical Co., Ltd. PER and MA were purchased from Fuchen Chemical Reagent, (Tianjin, China). HEDP was provided by Shandong Taihe Water Treatment Co., Ltd. (Shandong China). Urea was supplied by Zhiyuan Chemical Reagent (Tianjin, China). CS was purchased from Aoxing Bio-Science Technology Co., Ltd. (Zhejiang, China). Melamine pyrophosphate (MPP) was prepared in our laboratory.[19] All of these commercial materials were used directly without further purification.

Synthesis of HUMCS

First, CS (9.66 g) and urea (3.6 g, 0.06 mol) were dissolved in 300 mL of deionized water, and the solution was placed in an icebox at 0°C for 24 h. Second, after unfreezing, the aforementioned solution was fed into a three-necked flask equipped with a stirrer, a reflux condenser, and a glass stopper. Third, a solution of HEDP (12.36 g, 0.06 mol) in distilled water (100 mL) was added slowly to the three-necked flask, and the reaction temperature was simultaneously increased to 120°C. The reaction was carried out at 120°C for 2 h. Then, the reaction system temperature was set at 75°C, and the reaction was continued. When the system temperature was kept at 75°C, a solution of MA (7.56 g 0.06 mol), which was dissolved in hot water (200 mL), was injected into the three-necked flask drop by drop within 0.5 h. After further heating at reflux for 3 h, the reaction was completed. After direct hot filtration, washing with warm water, and drying at 90°C, the novel flame-retardant synergist, HUMCS, was obtained as a light yellow powder with a 93.6 wt % yield. Scheme 1 shows the synthetic route.

Preparation of the Flame-Retardant PP Samples

The IFR consisted of MPP and PER with a weight ratio of 2:1, and the total dosage of flame retardant was kept at 25 wt % in the IFR–PP composites. Then, HUMCS was added systematically to the IFR–PP composites as a synergist from 1 to 5 wt %. The detailed formulations of the samples are listed in Table I. All of the materials were dried in a vacuum oven at 80°C for 12 h before use. Then PP, MPP, PER, and HUMCS were melt-mixed in a twin-roll mill (XK-160, Shanghai Rubber Machinery Factory, China) for 15 min. The temperature of the mill was maintained at 175°C, and the roller speed was 40 rpm. The extruded strands were cut into pellets. Then, the composites were injected into standard testing bars with an injection-molding machine (PL860 Haitian Plastic Machinery Co., Ltd.,

Table I. Compositions of the Samples and Results from the LOI and UL-94 Tests

	Composition				UL-94			
Sample	PP (%)	IFR (%)[a]	HUMCS (%)	LOI (%)	First flame time (s)	Second flame time (s)	Dripping	Rating
PP	100	0	0	17.6	—	—	Yes	Failed
IFR-PP0	75	25	0	31.4	0	20	No	V-0
IFR-PP1	75	24	1	32.1	0	7	No	V-0
IFR-PP2	75	23	2	32.4	0	1	No	V-0
IFR-PP3	75	22	3	33.0	0	0	No	V-0
IFR-PP4	75	21	4	32.3	3	6	No	V-0
IFR-PP5	75	20	5	31.5	5	12	Yes	V-2

[a] IFR was composed of MPP and PER with a weight ratio of 2:1.

Ningbo, China) with a temperature profile of 180, 185, 190, 185, and 180°C, and the mold temperature was set at 40°C.

Characterization and Measurements

Fourier transform infrared (FTIR) spectra of the samples were recorded with KBr powder on a Nicolet FTIR 5700 spectrometer over the wave-number range from 500 to 4000 cm^{-1}.

^{31}P-NMR was performed on an Avance III 500 spectrometer (Bruker Biospin, Switzerland) at room temperature with $CDCl_3$ as the solvent and tetramethylsilane as an internal standard.

Thermogravimetric analysis (TGA) tests were carried out on a TG STA449C thermoanalyzer instrument (Netzsch, Germany) from 30 to 700°C at a heating rate of 10 K/min (nitrogen atmosphere, flow rate = 100 mL/min).

Microscale combustion calorimetry (MCC) tests were carried out on a GOVMARK MCC-2 machine according to ASTM D 7309-11. In this system, about 5-mg samples were heated to 750°C at a heating rate of 1 K/s and in a stream of nitrogen flowing at 80 cm^3/min.

Limiting oxygen index (LOI) testing was conducted on a JF-3 oxygen index instrument (Nanjing Jiangning Analysis Instrument, China) with sheet dimensions of 100 × 6.5 × 3 mm^3 according to ASTM D 2863.

Vertical burning ratings tests (UL-94) was performed on a vertical burning instrument (CZF-3, Nanjing Jiangning Analysis Instruments, China) with sheet dimensions of 130 × 13 × 3 mm^3 according to ASTM D 3801.

Tensile tests were completed on a universal experimental machine (CMT6104, MTS Systems Co., Ltd., China) in accordance with the procedures in GB/T 1040–1992 at an extension speed of 50 mm/min at room temperature. The specimens were dumbbell-shaped with a size of 160 × 10 × 4 mm^3. Five independent measurements were conducted, and the relative errors committed on each datum were reported as well.

Scanning electron microscopy (SEM) micrographs were obtained by an XL30 scanning electron microscope (Philips-FEI, The Netherlands) with a 25.0-kV beam voltage. The samples for the SEM micrographs of the intumescent char layer were residue left after the LOI tests. All of the samples were coated with a conductive gold layer.

RESULTS AND DISCUSSION

FTIR, ^{31}P-NMR, and TGA Characterization of the HUMCS

Figure 1 shows the FTIR spectra of the CS and HUMCS. Compared with the FTIR spectra of CS, the FTIR curve of the HUMCS showed some changes. The characteristic broad band responsible for the amino, imino, and hydroxyl stretching in the curve of HUMCS was shifted from 3430 to 3390 cm^{-1}. A new wide and strong absorption peak appeared at 3146 cm^{-1}, and it was ascribed to the vibration absorption of -NH_3^+. In addition, another absorption peak for -NH_3^+ was found at 1535 cm^{-1}; this implied that some amino groups in MA underwent a reaction to form phosphorylamide groups.[20] Moreover, the three peaks at 1020, 1100, and 1150 cm^{-1} were attributed to stretching vibrations of the P-O structure, such as P-O-C and P-O-H. This indicated that the reaction occurred between CS and HEDP.

Figure 2 presents the ^{31}P-NMR spectra of the HUMCS. According to Jacopin et al.,[21] the ^{31}P-NMR spectra of HEDP had one single peak around 20 ppm. However, two new resonances were

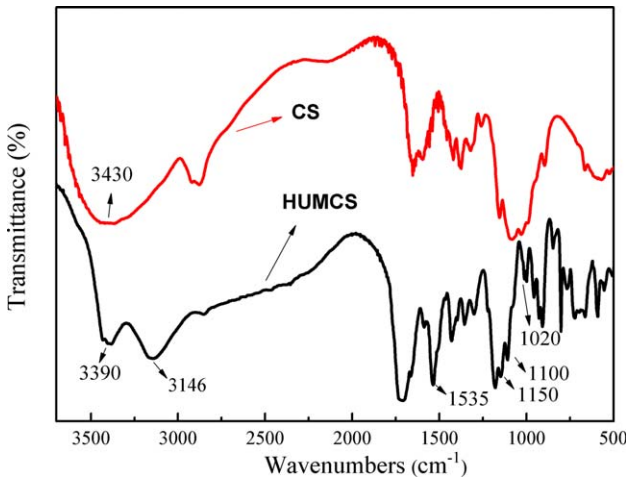

Figure 1. FTIR spectra of CS and HUMCS. [Color figure can be viewed in the online issue, which is available at wileyonlinelibrary.com.]

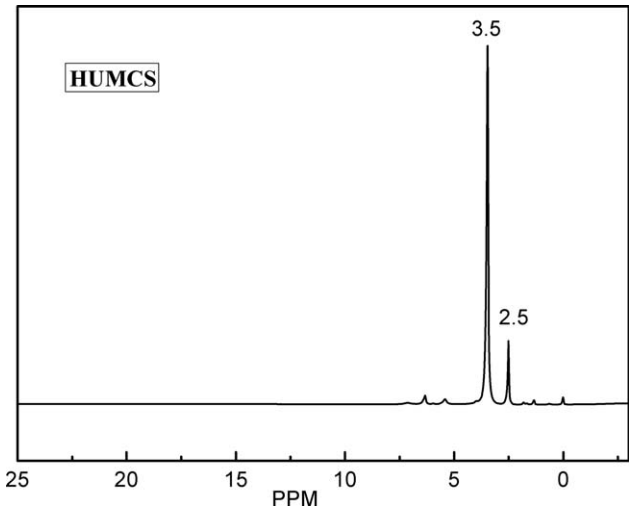

Figure 2. ^{31}P-NMR spectra of HUMCS.

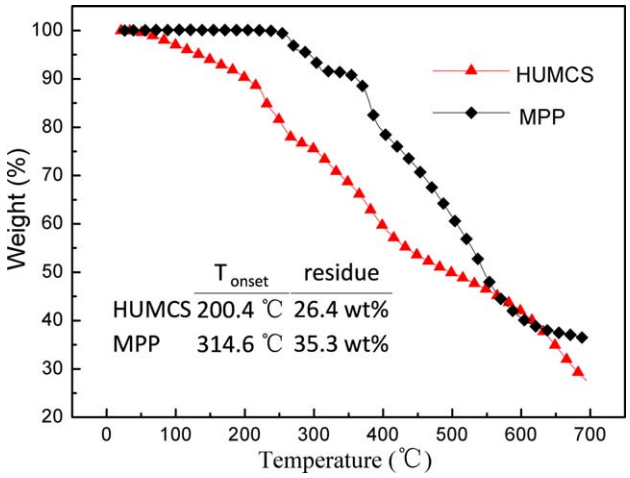

Figure 4. TGA curves of HUMCS and MPP in air. [Color figure can be viewed in the online issue, which is available at wileyonlinelibrary.com.]

found for HUMCS; this suggested that HEDP reacted with MA and CS, respectively. The FTIR and NMR results prove that the synthesis of HUMCS was successful.

Figure 3 exhibits the TGA curves of HUMCS and MPP, which were obtained under a nitrogen atmosphere. As shown, HUMCS had two degradation stages. The onset decomposition temperature (T_{onset}) was around 200°C. This was probably related to the chemical reactions of dehydration, the release of ammonia, and the loss of absorbed water. The second decomposition phase occurred at about 300°C; this may have corresponded to the degradation of the polysaccharide structure and the formation of a series of lower fatty acids.[22,23] Although HUMCS had a worse thermal stability as compared to MPP, but its char residue at 700°C was much higher than that of MPP at nearly 50 wt %.

The thermal behaviors of HUMCS and MPP were analyzed further in air, as shown in Figure 4. It was interesting to find that HUMCS and MPP showed different changes in air than in nitrogen. Before 550°C, HUMCS showed similar thermal degradation processes in two different atmospheres. However, it showed a quick weight loss in air between 550 and 700°C with a residue of only 26.4 wt %; this was 21.2 wt % less than that in a nitrogen atmosphere. This may have been due to the residual crosslinked degradation of CS.[24] On the other hand, the residue of MPP showed barely any changes under the two different conditions. From the previous discussion, we concluded that the decomposition of HUMCS was more rapid than that of MPP in the low-temperature range, but it had better charring properties in the high-temperature region.

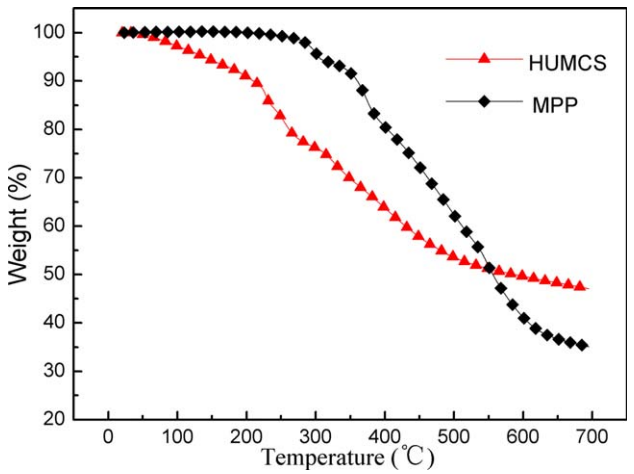

Figure 3. TGA curves of HUMCS and MPP under a nitrogen atmosphere. [Color figure can be viewed in the online issue, which is available at wileyonlinelibrary.com.]

Flame Retardancy and Thermal Stability

LOI and UL-94 tests are the most common way to investigate the flame retardancy of plastics. The detailed results of all of the samples are shown in Table I; they include the first flame time, second flame time, and dripping behavior. A 25 wt % loading of IFR obviously improved the LOI value of PP, which ascended from 17.6 to 31.4. In addition, the LOI values of the PP/IFR/HUMCS composites increased further with increasing loading of HUMCS, and it reached a maximum value at 33%; this suggested that HUMCS improved the flame retardancy of the IFR–PP composites. In the UL-94 test, the flames were self-

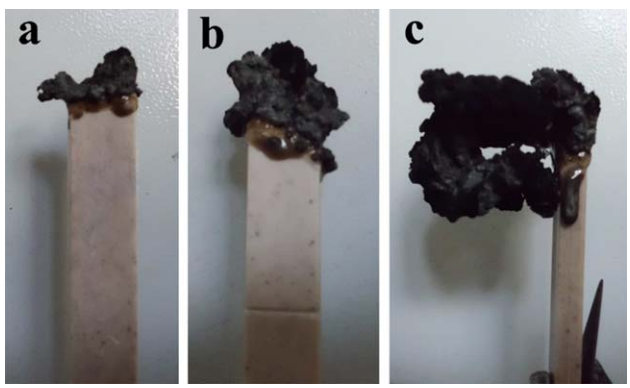

Figure 5. Digital photos of IFR–PP3 after the LOI tests. O_2 was (a) 30, (b) 32, and (c) 33%. [Color figure can be viewed in the online issue, which is available at wileyonlinelibrary.com.]

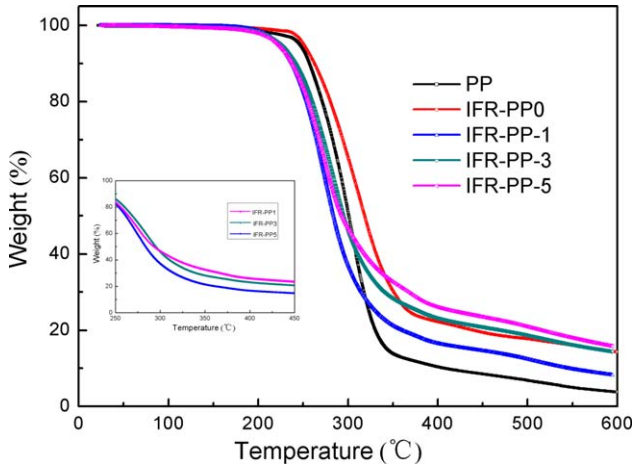

Figure 6. TG curves of the PP and IFR–PP composites in air. [Color figure can be viewed in the online issue, which is available at wileyonlinelibrary.com.]

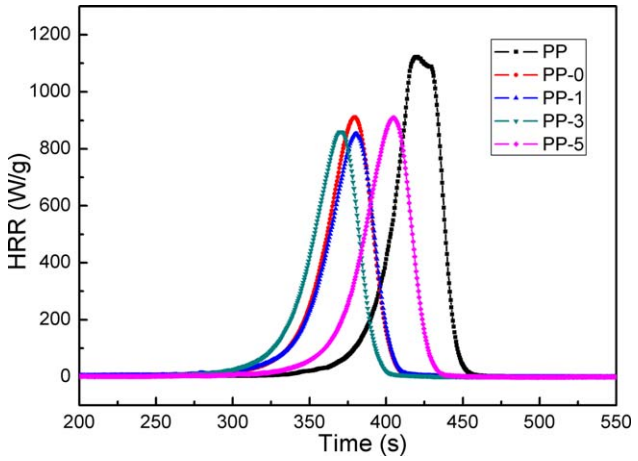

Figure 8. HRR curves of the PP and IFR–PP composites. [Color figure can be viewed in the online issue, which is available at wileyonlinelibrary.com.]

extinguished more rapidly, and the second flame time became much shorter after the addition of HUMCS. However, the LOI values of IFR–PP4 and IFR–PP5 declined afterward. This may have been due to the low degradation temperature of HUMCS, and the overloading of HUMCS accelerated the decomposition of the PP/IFR/HUMCS composites. In conclusion, HUMCS played a unique role in the system, and the optimal synergistic effect was based on a just right formulation between the HUMCS and IFR–PP composites. When the content of HUMCS was 3 wt % and that of IFR was 22 wt %, the LOI value of IFR–PP3 was 33%, and it achieved a V-0 rating in the UL-94 test. These results were compatible with the analyses of Figures 3, 8, and 11 (shown later).

The digital photos of the IFR–PP3 specimen after the LOI tests are shown in Figure 5. As shown, IFR–PP3 possessed obvious intumescent char, which was formed during burning with increasing O_2 content. Few char layers were formed when the O_2 contents were 31 and 32%, as shown in corresponding sample in Figure 5(a,b), respectively, and both samples were rapidly self-extinguished. However, notable intumescent char layers were found in sample c during the burning process when the O_2 content in the atmosphere was 33%.

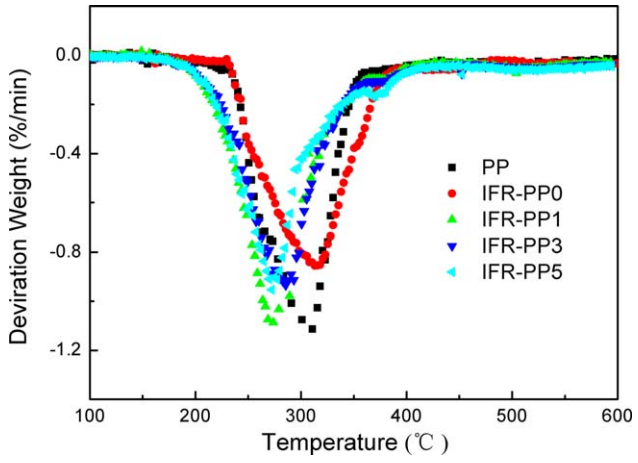

Figure 7. DTG curves of the PP and IFR–PP composites under an air atmosphere. [Color figure can be viewed in the online issue, which is available at wileyonlinelibrary.com.]

To further investigate the interaction between the HUMCS and IFR–PP composites, thermogravimetry (TG) and derivative thermogravimetry (DTG) curves of PP, IFR–PP0, IFR–PP1, IFR–PP3, and IFR–PP5 were obtained, as shown in Figures 6 and 7, respectively, and the corresponding data are given in Table II. The neat PP decomposed rapidly from 240 to 350°C, and its decomposition was almost completed at 600°C with a little residual char (3.8 wt %). As shown in Figures 6 and 7, IFR–PP0 possessed more thermal stability than pure PP because of the incorporation of IFR. However, both the 5% weight loss temperature ($T_{-5wt\ \%}$) and the maximum weight loss temperature (T_{max}) of the IFR–PP composites with HUMCS were lower than those of pure PP. This indicated the addition of HUMCS accelerated the decomposition of the IFR–PP samples in air below 300°C. Meanwhile, the thermal oxidative behaviors of the IFR–PP composites with HUMCS were similar under these experimental conditions, but IFR–PP3 showed a higher thermal stability than IFR–PP1 and IFR–PP5. On the other hand, the char residue of the flame-retardant PP composites at high temperature increased with increasing HUMCS content. This proved that HUMCS had a good synergistic effect with IFR to promote the formation of char in the IFR–PP composites.

Table II. Thermal Degradation Data under Air by TGA

Sample	$T_{-5wt\ \%}$ (°C)	T_{max} (°C)	Char residue at 600°C (wt %)
PP	246.4	310.7	3.8
IFR-PP0	250.6	317.3	14.3
IFR-PP1	223.2	268.9	8.3
IFR-PP3	225.0	286.7	14.5
IFR-PP5	221.3	276.1	15.8

Table III. Combustion Parameters Obtained from MCC

Sample	pHRR (W/g)	HRC (J g^{-1} K^{-1})	THR (kJ/g)
PP	1136	1141	43.8
IFR-PP0	917	903	35.1
IFR-PP1	859	868	34.0
IFR-PP3	860	869	33.8
IFR-PP5	913	940	35.5

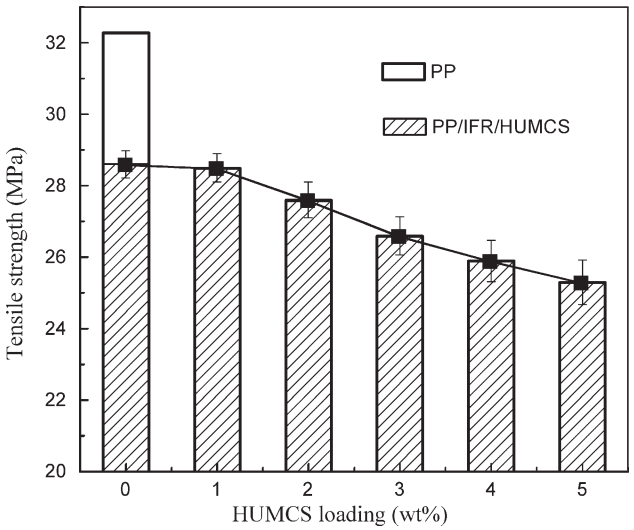

Figure 9. Effect of the HUMCS loading on the tensile strength of the IFR–PP composites.

MCC is an effective thermal combustion analysis instrument for small quantities of samples. Parameters, including the peak heat-release rate (pHRR), total heat release (THR), and heat-release capacity (HRC), can be obtained to evaluate the flammability of the samples.

The heat-release rate (HRR) curves of the PP and IFR–PP composites are shown in Figure 8, and the corresponding combustion data are presented in Table III. HRR has been recognized as one of the most important parameters used to characterize a fire, and low values of pHRR are an indication of low flammability. Pure PP is a flammable polymer with a sharp pHRR. For IFR–PP0, the pHRR value was greatly reduced from 1136 to 903 J g^{-1} K^{-1} in comparison with that of neat PP because of the flame retardancy of IFR. In the case of IFR–PP1 and IFR–PP3, the addition of HUMCS decreased the pHRR values to 859 and 860 J g^{-1} K^{-1}, respectively. This indicated a good synergistic effect between HUMCS and IFR. However, the pHRR value of IFR–PP5 increased to the same level as that of IFR–PP0; this suggested that the redundant HUMCS counteracted the synergistic effect between HUMCS and IFR. This might have been caused by the competitive relationship between the promotion of char formation and the acceleration of degradation, which was in accordance with the conclusions of the TGA of HUMCS.

From the previous discussions, we concluded that HUMCS played a dual role by accelerating decomposition and promoting char formation on the IFR–PP composites. So the appropriate addition of HUMCS for the IFR–PP composites was needed to achieve better flame-retardant and thermal stability properties.

Tensile Properties and Morphological Structures of the Composites

The effects of the HUMCS loading on the tensile strength of the IFR–PP composites are presented in Figure 9. As shown, the tensile strength of the neat PP decreased from 32.3 to 28.5 MPa after the addition of 25 wt % IFR. This was mainly because of the poor compatibility between the IFR and the PP matrix. However, with increasing addition of HUMCS, the tensile strengths of the PP/IFR/HUMCS composites deteriorated even more. The tensile strength of IFR–PP1 remained at the same level with that of IFR–PP0, but the process addition of 5 wt % HUMCS decreased the tensile strength to 3.2 MPa. This indicated that the compatibility of HUMCS was worse than that of IFR.

The tensile properties were correlated with the microstructures of composites. So, the morphologies of IFR–PP0 and IFR–PP3 observed by SEM measurement are given in Figure 10. As shown in Figure 10(a) (the micrographs of IFR–PP0), few uniform holes were observed in the IFR–PP composites. However, as shown in Figure 10(b) (the samples of IFR–PP3), lots of flaws were dispersed in the matrix. According to the analysis in Figure 3, the decomposition of HUMCS might have released some of the absorbed water and ammonia at low temperature; this would have resulted in poor compatibility between the HUMCS and IFR–PP composites. In this case, the tensile properties of the PP/IFR/HUMCS composites must have decreased.

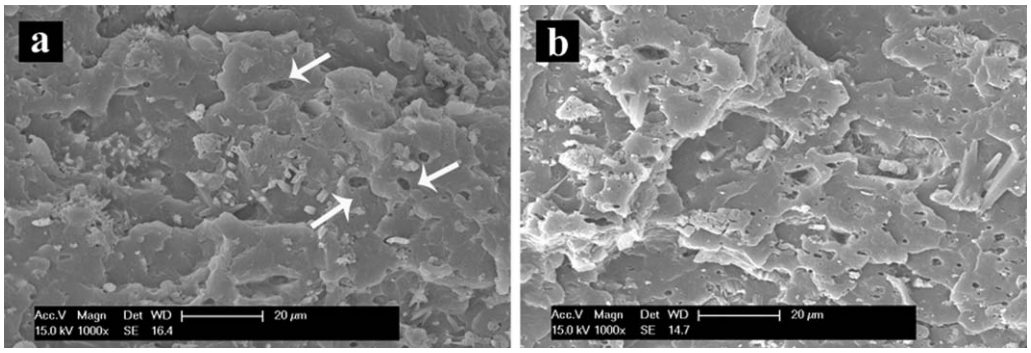

Figure 10. SEM micrographs for (a) IFR–PP0 and (b) IFR–PP3.

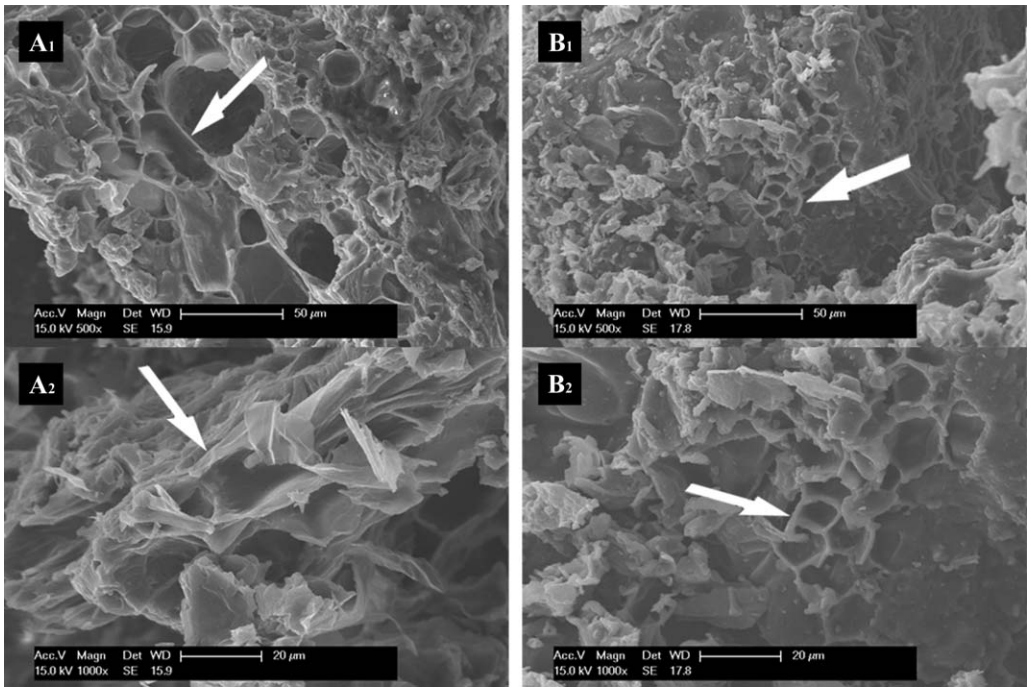

Figure 11. SEM micrographs of the residues of inner surfaces of (A_1,A_2) IFR–PP0 and (B_1,B_2) IFR–PP3.

Structural Analysis of the Char Residue

It is popularly accepted that the formation of dense and multicellular intumescent charred layers during combustion can protect a substrate material from combustion, so a dense multicellular char is an essential factor in the improvement of the flame retardancy of IFR–PP composites. Figure 11 shows the SEM images of the micrographs of the char residues after the LOI test. A cellular structure was found in both char residues, but compared to the samples without HUMCS [Figure 11(A1,A2)], the char residue of the sample with 3 wt % HUMCS [Figure 11(B1,B2)] had smaller and more compact cellular walls; this slowed down the action of the heat flux and retarded the mass transfer between the gaseous and condensed phases. This result was in accordance with the LOI tests, UL-94 tests, MCC tests, TGA, and DTG analysis of the IFR–PP composites.

CONCLUSIONS

A novel CS-based charring agent, HUMCS, was successfully synthesized in a CS/urea solution. Then, it was applied to improve the flame-retardant properties of the IFR–PP composites. Although it decreased the tensile properties of the IFR–PP composites, its positive impact on the flammability performance was obvious. TGA revealed that HUMCS decomposed at low temperatures, but it had good charring properties in the high-temperature region. The LOI value of the IFR–PP3 increased to 33.0; that is, that the LOI value increased by 1.6 units compared to that of IFR–PP0. The results of MCC indicate that the appropriate addition of HUMCS decreased the pHRR, HRC, and THR. Furthermore, from the analysis of the SEM images of the char residues, we deduced that a dense and compact multicell char was formed because of the synergistic effect of HUMCS. In summary, all of the previous tests confirmed that the appropriate addition of HUMCS had a good synergistic effect with IFR by promoting char formation.

ACKNOWLEDGMENTS

This work was supported by the Scientific and Technological Innovation Project of Fujian Province (contract grant number 2010H2005) and the Science and Technology Planning Project of Fuzhou (contract grant number 2013-G-92).

REFERENCES

1. Liu, Y.; Zhao, J.; Deng, C. L.; Chen, L.; Wang, D. Y.; Wang, Y. Z. *Ind. Chem. Res.* **2011**, *50*, 2047.
2. Cao, K.; Wu, S. L.; Qiu, S. L.; Li, Y.; Yao, Z. *Ind. Chem. Res.* **2012**, *52*, 309.
3. Lai, X. J.; Zeng, X. R.; Li, H.; Yin, C.; Zhang, H.; Liao, F. *J. Appl. Polym. Sci.* **2012**, *125*, 1758.
4. Gao, F.; Tong, L.; Fang, Z. *Polym. Degrad. Stab.* **2006**, *91*, 1295.
5. Lai, X. J.; Zeng, X. R.; Li, H.; Liao, F.; Yin, C.; Zhang, H. *Polym. Compos.* **2012**, *33*, 35.
6. Feng, J.; Zhang, X.; Ma, S. *Ind. Chem. Res.* **2013**, *52*, 2784.
7. Zhan, J.; Song, L.; Nie, S.; Hu, Y. *Polym. Degrad. Stab.* **2009**, *94*, 291.
8. Li, B.; Xu, M. *Polym. Degrad. Stab.* **2006**, *91*, 1380.
9. Laufer, G.; Kirkland, C.; Cain, A. A.; Grunlan, J. C. *Appl. Mater. Interfaces* **2012**, *4*, 1643.
10. Tahlawy, K. E. *J. Text. Inst.* **2008**, *99*, 185.
11. Shahid, U. I.; Shahid, M.; Mohammad, F. *Ind. Chem. Res.* **2013**, *52*, 5245.

12. Sogias, I. A.; Khutoryanskiy, V. V.; Williams, A. C. *Macromol. Chem. Phys* **2010**, *211*, 426.
13. Hu, S.; Song, L.; Pan, H.; Hu, Y. *Ind. Chem. Res.* **2012**, *51*, 3663.
14. Hu, S.; Song, L.; Pan, H.; Hu, Y. *Therm. Anal. Calorim.* **2012**, *112*, 859.
15. Chenite, A.; Gori, S.; Shive, M.; Desrosiers, E.; Buschmann, M. D. *Carbohydr. Polym.* **2006**, *64*, 419.
16. Tsaih, M. L.; Chen, R. H. *Int. J. Biol. Macromol.* **1997**, *20*, 233.
17. Teli, M. D.; Sheikh, J.; Bhavsar, P. *Int. J. Biol. Macromol.* **2013**, *54*, 125.
18. Vellingiri, K.; Ramachandran, T.; Senthilkumar, M. *Nano Lett.* **2013**, *5*, 519.
19. Jiao, C. M.; Chen, X. L. *Polym. Eng. Sci.* **2010**, *50*, 767.
20. Wang, X. H.; Ma, J. B.; Wang, Y. N.; He, B. L. *Carbohydr. Res.* **2001**, *22*, 2247.
21. Jacopin, C.; Sawicki, M.; Plancque, G.; Doizi, D.; Taran, F.; Ansoborlo, E.; Amekraz, B.; Moulin, C. *Inorg. Chem.* **2003**, *42*, 5015.
22. Wang, X. L.; Huang, Y.; Zhu, J.; Pan, Y. B.; He, R.; Wang, Y. Z. *Carbohydr. Res.* **2009**, *344*, 801.
23. Hu. S.; Song, L.; Pan, H.; Hu, Y.; Gong, X. *Therm. J. Anal. Appl. Pyrolysis* **2012**, *97*, 109.
24. Rinaudo, M. *Prog. Polym. Sci.* **2006**, *31*, 603.